Theoretical Evaluation of Hybrid Simulation Applied to Continuous Plate Structures

Ahmed A. Bakhaty[1]; Sanjay Govindjee[2]; and Khalid M. Mosalam, M.ASCE[3]

Abstract: Hybrid simulation is a popular experimental technique whereby only part of a system is physically realized and the remainder is modeled in a computer with a set of actuators and sensors to connect the two subsystems. While the methodology is common, it lacks a theoretical structure that ensures users are getting valid simulation results of the entire system. Further, little attention has been paid to distributed mass systems and those that do not have a beam/column like topology. This work examines three basic issues: (1) an abstract geometric scheme is proposed by which one can reason about hybrid simulation systems and their underlying errors; (2) systems with distributed mass are explicitly considered; and (3) the model system utilized in this study has a distinctly nonbeam/column like system, namely, a Kirchhoff-Love plate with a continuous one-dimensional hybrid system interface. It is demonstrated that such systems are generally viable only below the first fundamental frequency of the system. Furthermore, it is shown that there is a tendency to accumulate global errors, relative to the classical solution, at the slightest introduction of any interface matching error but that these errors are mostly insensitive to further increase in mismatch. Finally, it is found that the different substructures of the systems are subject to resonant excitation at their own independent natural frequencies in addition to those of the complete hybrid system. **DOI: 10.1061/(ASCE)EM.1943-7889.0001157.**

Author keywords: Hybrid simulation; Real-time hybrid simulation; Elastic plate theory; Error analysis; Experimental error.

Introduction

Hybrid testing is a class of simulation techniques that aims to overcome the limitations of pure experimentation and pure numerical simulation by using a scheme that combines the two with actuators and sensors. The concept is to test only part of the system and numerically simulate the rest. Of these methods, hybrid simulation (Schellenberg 2008), formerly called pseudodynamic testing (Shing and Mahin 1984), is the most prominent. In this method, a system is split into a computational substructure (numerical model) and a physical substructure (a specimen in the laboratory) and the governing equations of motions of the system are solved with a time-stepping algorithm. At each time step, displacements computed by the numerical algorithm are imposed via actuators on the physical substructure, whose response is measured by sensors and communicated back to update the system variables and march forward to the next time step. Naturally inherent errors exist in the technique that include time integration errors, control errors, interface splitting errors, and random signal errors, which can further be classified as either systematic or random errors. Although not a necessary requirement, hybrid simulation can be performed in real time (Mosalam and Günay 2014; Günay and Mosalam 2014).

Originally conceived in the 1970s as an online testing method for evaluating the nonlinear response of structures subjected to earthquake excitation (Takanashi et al. 1975), the technique has seen significant development over the years. Such developments have taken the method from simply using the numerical substructure for modeling only the mass and damping of the system to numerical substructures that are full finite-element models communicating in real time with the physical specimen in the laboratory (Thewalt and Mahin 1987; Igarashi et al. 1992; Nakashima 2001; Elkhoraibi and Mosalam 2007). Much attention has been devoted to studying the source and effect of the inherent errors in hybrid testing and proposing mitigation techniques (Shing and Mahin 1987; Horiuchi and Konno 2001; Ahmadizadeh et al. 2008), but little work has been dedicated to understanding the theoretical limitations of the technique in the presence of these errors. In other words, what are the best possible results that can be achieved with hybrid testing, as compared to the true response of the real system? To address this issue, this study presents a theoretical framework for the general assessment and evaluation of hybrid simulation (HS)—a form of hybrid testing of current interest (Schellenberg 2008).

The objective of this study is to characterize the *theoretical* performance of HS, applied to platelike structures with distributed mass, by understanding how the errors influence the global response of the system. In order to have a completely controlled setting for analyzing the HS technique, a purely theoretical system will be utilized in which both the traditional physical and computational parts are mathematical models. The transfer system, i.e., the actuators, sensors, data acquisition, and reaction frame, is also represented by simple mathematical models. In this manner, attention can be focused on the essential error associated with a system possessing a split interface and on understanding the inherent error associated with imperfect interface splitting. This provides a true estimate of the best possible realistic error targets for a hybrid system.

The solution to the governing equations of a system (e.g., equations of motion of a mechanical system) can be considered as a trajectory in an L^2 space. The associated hybrid system obeys

[1]Graduate Student, Dept. of Civil and Environmental Engineering, Univ. of California, Berkeley, CA 94720-1710. E-mail: abakhaty@berkeley.edu

[2]Professor, Dept. of Civil and Environmental Engineering, 779 Davis Hall, Univ. of California, Berkeley, CA 94720-1710 (corresponding author). E-mail: govindjee@ce.berkeley.edu

[3]Taisei Professor of Civil Engineering, Dept. of Civil and Environmental Engineering, 723 Davis Hall, Univ. of California, Berkeley, CA 94720-1710. E-mail: mosalam@ce.berkeley.edu

Note. This manuscript was submitted on July 7, 2015; approved on June 23, 2016; published online on August 8, 2016. Discussion period open until January 8, 2017; separate discussions must be submitted for individual papers. This paper is part of the ***Journal of Engineering Mechanics***, © ASCE, ISSN 0733-9399.

the same governing equations of the real system in the respective domains (physical and computational), but are coupled at the interface by introduced constraints. The solutions in each domain are themselves trajectories in an L^2 space, and thus the trajectory of the sum space of the two domains may be compared with the trajectory of the true solution using an appropriate metric in the inner product space. Thus the error can be defined as the L^2 norm of the difference in trajectories of the true and hybrid solutions.

The proposed model system will be a Kirchhoff-Love thin plate in which all equations will be analytically solved and thus the analysis herein represents the best possible case obtainable in HS. It is emphasized that the true continuum problem is being treated, not a lumped mass approximation. Because the proposed system is two dimensional, the present analysis will also explicitly deal with the issues associated with hybrid system interfaces that are geometrically continuous (as opposed to isolated points). One of the central aims of this work is to understand the similarities and differences of such true two-dimensional systems to one-dimensional systems such as beam flexure that were earlier investigated using the same conceptual framework by Drazin et al. (2015). Additionally, this work examines more-generalized error models—those that are frequency dependent.

Theoretical Framework

Consider a reference mechanical system with domain $\mathcal{D}$, depicted in Fig. 1(a), whose response is determined from a governing set of equations

$$F[\mathbf{u}(\mathbf{x},t)] = \mathbf{0}, \qquad \mathbf{x} \in \mathcal{D} \tag{1a}$$

$$\mathbf{u}(\mathbf{x},t) = \bar{\mathbf{u}}, \qquad \mathbf{x} \in \partial\mathcal{D} \tag{1b}$$

where $\mathbf{u}$ = characteristic quantity (e.g., displacements, velocities, accelerations, etc.); $\bar{\mathbf{u}}$ = imposed value of that quantity on the boundary; $\mathbf{x}$ = position in space; and t = time. The domain is next separated into two subdomains denoted by $\mathcal{P}$ and $\mathcal{C}$, which represent the physical and computational substructures, respectively, as depicted in Fig. 1(b). Without loss of generality, only two subdomains are considered for simplicity, but HS may have multiple physical and computational substructures (Elkhoraibi and Mosalam 2007). The response of each domain, determined by Eqs. (1*a*) and (1*b*) applied locally to $\mathcal{P}$ and $\mathcal{C}$, is given by

$$\hat{\mathbf{u}} = \begin{cases} \hat{\mathbf{u}}_p(\mathbf{x},t) & \text{if } \mathbf{x} \in \mathcal{P} \\ \hat{\mathbf{u}}_c(\mathbf{x},t) & \text{if } \mathbf{x} \in \mathcal{C} \end{cases} \tag{2}$$

where the superposed hats ($\hat{\bullet}$) = quantities in the hybrid system. In addition to the boundary conditions on the reference system, applied accordingly to the hybrid system, there must also be conditions on the interface boundaries, $\mathcal{I}_p$ and $\mathcal{I}_c$. Physically, these are provided by the sensor and actuator system. These conditions are modeled here by boundary functions $\mathbf{g}_p$ and $\mathbf{g}_c$, respectively, for $\mathcal{P}$ and $\mathcal{C}$

$$\hat{\mathbf{u}}_p(\mathbf{x}_p,t) = \mathbf{g}_p(\mathbf{x}_p,t), \qquad \mathbf{x}_p \in \mathcal{I}_p \tag{3a}$$

$$\hat{\mathbf{u}}_c(\mathbf{x}_c,t) = \mathbf{g}_c(\mathbf{x}_c,t), \qquad \mathbf{x}_c \in \mathcal{I}_c \tag{3b}$$

A constraint is imposed on corresponding boundary functions at the interface to join the two components of the hybrid system. This constraint takes into consideration the imperfect dynamics of the hybrid system, such as time delays between the two components or tracking errors. This relation may be posed as

$$\underline{D}[\hat{\mathbf{u}}_c]|_{\mathcal{I}_c} = \underline{E}\,\underline{D}[\hat{\mathbf{u}}_p]|_{\mathcal{I}_p} \tag{4}$$

where $\underline{D}[\bullet]$ = operator that provides the necessary boundary functions at the interface from the displacements, $\hat{\mathbf{u}}_p$ and $\hat{\mathbf{u}}_c$; and $\underline{E}$ = error operator that applies a mismatch (or error) between corresponding boundary functions generated by $\underline{D}[\bullet]$. One such form, representative of time delay and tracking error as encountered in HS due to finite communication time of the actuator system (Horiuchi et al. 1999; Conte and Trombetti 2000), is presented as follows:

$$g_p^k = e^{i\Omega d_k} g_c^k (1+\varepsilon_k) \tag{5}$$

where Ω represents the frequency of excitation, but is not directly the frequency of excitation, ω. Later, Ω will be redefined as a dimensionless excitation of frequency, and thus, d_k will be dimensionless. Throughout, $i = \sqrt{-1}$ is the imaginary unit, and the parameters ε_k and d_k represent the magnitude and phase of the error, respectively, in the kth boundary quantity, $g_{(\bullet)}^k$. It is emphasized that the solution to the governing equations in each domain can be derived exactly without the use of any numerical schemes as is the case with HS and thus the only source of error in the analysis comes from the constraint presented in Eq. (5).

If so desired, Eq. (5) may be modified to include the effect of frequency dependence on the error. Physically speaking, a controller will have more difficulty keeping up while operating at higher frequencies and larger error is observed when compared to lower frequencies (Conte and Trombetti 2000; Günay and Mosalam 2015). Making use of the generalized logistic function (Richards 1959), a simple frequency-dependent error model may be expressed as

$$\varepsilon_k(\omega) = \frac{\varepsilon_{k0}}{[1+e^{(\omega_{k0}-\omega)}]^2} \tag{6}$$

where for the kth quantity; ε_{k0} = maximum error magnitude reached asymptotically at high frequencies; ω = excitation frequency; and ω_{k0} = frequency of maximum growth rate. The analysis herein is limited to an error model as given by Eq. (5) with a later

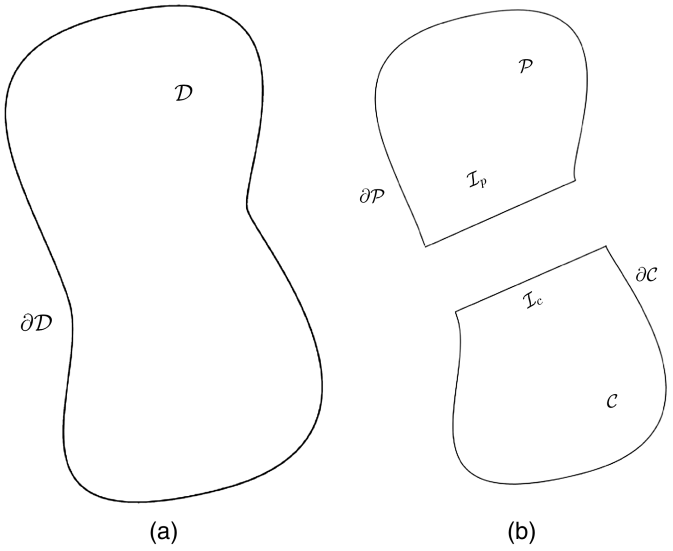

Fig. 1. Theoretical concept of hybrid simulation: (a) domain of system to be simulated; (b) hybrid domain of system to be simulated

J. Eng. Mech., 2016, 142(12): 04016093

modification for Eq. (6) but the selection of an appropriate interface error model is not unique.

Application to Kirchhoff-Love Thin Plate

To make the proposed general framework concrete, it will now be applied it to a classical problem in continuum mechanics with a wide array of important engineering applications: a simply supported Kirchhoff-Love $a \times b$ plate (Timoshenko 1959) subjected to a time harmonic edge bending moment as shown in Fig. 2.

The plate is considered linear-elastic and isotropic with infinitesimal kinematics. For a treatment with damping, the reader is referred to the work of Drazin et al. (2015). The governing equation of motion is, e.g., Graff (1975)

$$D\nabla^4 w + \rho h \frac{\partial^2 w}{\partial t^2} = 0 \tag{7}$$

where w = out-of-plane displacement; $\nabla^4(\bullet)$ = biharmonic operator; and $D = Eh^3/12(1-\nu^2)$ = bending stiffness for Young's modulus, E; Poisson's ratio, ν; and plate thickness, h. The boundary conditions are simply supported with the addition of a harmonic edge bending moment at $y = b$

$$-D\frac{\partial^2 w}{\partial y^2}\bigg|_{y=b} = \bar{M} e^{i\omega t} \tag{8}$$

where $\bar{M}$ = magnitude of the applied bending moment per unit length; and ω = harmonic driving frequency. A solution in the spirit of Lévy (Timoshenko 1959) is given as

$$w(x,y,t) = \sum_{m=1}^{\infty} Y_m(y)\sin(\alpha_m x) e^{i\omega t} \tag{9}$$

where $\alpha_m = m\pi/a$. The selection of a Fourier series in only one direction is convenient for the one-sided excitation (Fig. 2) and is known to have faster convergence than a traditional double Fourier series solution (Taylor and Govindjee 2004). Eq. (9) results in a fourth-order ordinary differential equation in Y_m after substitution into Eq. (7) which can be solved, with the proper boundary conditions, to give a final result that is consistent with the one presented by Gorman and Sharma (1976)

$$\begin{aligned} w(x,y,t) = &\sum_{m=1,3,\ldots}^{m_c} \frac{4\bar{M}}{m\pi D(\gamma_1^2+\gamma_2^2)}\sin(\alpha_m x)\left[\frac{\sin(\gamma_2 y)}{\sin(\gamma_2 b)} - \frac{\sinh(\gamma_1 y)}{\sinh(\gamma_1 b)}\right] e^{i\omega t} \\ &+ \sum_{m=m_c+1,m_c+3,\ldots}^{m_r} \frac{4\bar{M}}{m\pi D(\gamma_1^2-\gamma_2^2)}\sin(\alpha_m x)\left[b\coth(\gamma_1 b)\frac{\sinh(\gamma_1 y)}{\sinh(\gamma_1 b)} - y\frac{\cosh(\gamma_1 y)}{\sinh(\gamma_1 b)}\right] e^{i\omega t} \\ &+ \sum_{m=m_r+1,m_r+3,\ldots}^{\infty} \frac{2\bar{M}}{m\pi D\gamma_1}\sin(\alpha_m x)\left[\frac{\sinh(-\gamma_2 y)}{\sinh(-\gamma_2 b)} - \frac{\sinh(\gamma_1 y)}{\sinh(\gamma_1 b)}\right] e^{i\omega t} \end{aligned} \tag{10}$$

where $\gamma_1 = \sqrt{\beta^2+\alpha_m^2}$, $\gamma_2 = \sqrt{|\beta^2-\alpha_m^2|}$, $\beta^4 = \rho h\omega^2/D$, and ρ = mass density of the material. The parameters m_r and m_c are defined such that $\alpha_m^4 > \beta^4$ for $m \le m_c$, $\alpha_m^4 = \beta^4$ for $m_c < m \le m_r$, and $\alpha_m^4 > \beta^4$ for $m > m_r$. The constant coefficient ordinary differential equation (ODE) has a characteristic polynomial with roots that vary depending on α_m. This requires a solution [Eq. (10)] that accounts for the imaginary, repeated, and real roots. Eq. (10) represents the solution to the real plate. In the hybrid system, each subsystem, $\mathcal{P}$ and $\mathcal{C}$, also has a solution of the form given in Eq. (9). The solution for the generalized coefficients, however, is more involved due to the boundary conditions at the splitting interface. The reader is referred to Bakhaty et al. (2014) for a detailed expressions.

The boundary functions introduced in Eqs. (3*a*) and (3*b*) are not defined explicitly but can be determined from the constraints presented in Eq. (5). The boundary functions at the splitting interface for the $\mathcal{P}$ domain per Eq. (3*a*) can be expressed in Fourier form as

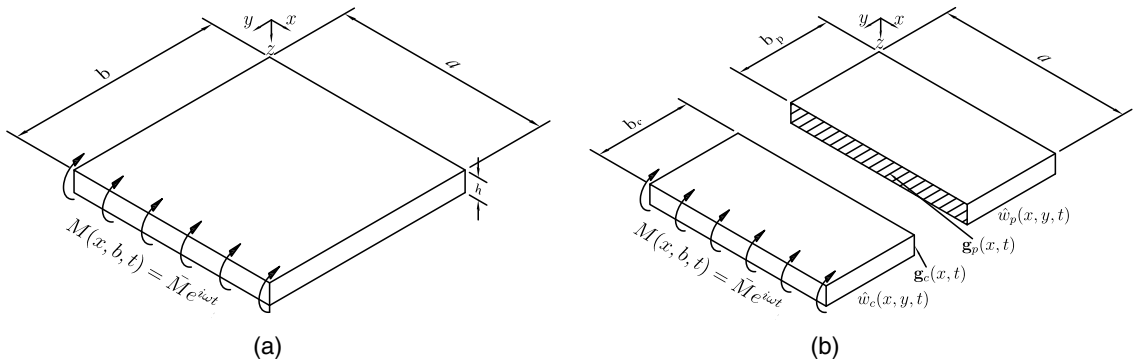

Fig. 2. Kirchhoff-Love simply supported plate subjected to a harmonic edge bending moment: (a) true formulation; (b) hybrid formulation

J. Eng. Mech., 2016, 142(12): 04016093

$$\hat{w}_p(x, b_p, t) = g^w_p(x, t) = \sum_{m=1,3,\ldots}^{\infty} \Gamma^w_{pm} \sin(\alpha_{pm} x) e^{i\omega t} \tag{11a}$$

$$\left.\frac{\partial \hat{w}_p}{\partial y}\right|_{y=b_p} = g^\theta_p(x, t) = \sum_{m=1,3,\ldots}^{\infty} \Gamma^\theta_{pm} \sin(\alpha_{pm} x) e^{i\omega t} \tag{11b}$$

where $g^w_{(\bullet)}$ and $g^\theta_{(\bullet)}$ = boundary functions representing the displacement and rotation at the splitting interface, respectively, and $\Gamma^w_{(\bullet)m}$ and $\Gamma^\theta_{(\bullet)m}$ = respective Fourier coefficients. The corresponding boundary functions for the $\mathcal{C}$ domain are

$$\tilde{w}_c(x, b_c, t) = g^w_c(x, t) = \sum_{m=1,3,\ldots}^{\infty} \Gamma^w_{cm} \sin(\alpha_{cm} x) e^{i\omega t} \tag{12a}$$

$$\left.\frac{\partial \tilde{w}_c}{\partial \tilde{y}}\right|_{\tilde{y}=b_c} = g^\theta_c(x, t) = \sum_{m=1,3,\ldots}^{\infty} \Gamma^\theta_{cm} \sin(\alpha_{cm} x) e^{i\omega t} \tag{12b}$$

The coordinates b_p and b_c are shown in Fig. 2(b) and a local coordinate, $\tilde{y} = b - y$, is introduced to the $\mathcal{C}$ domain in Eqs. (12*a*) and (12*b*) for convenience, with corresponding displacement $\tilde{w}_c(x, \tilde{y}, t) = \hat{w}_c(x, b - \tilde{y}, t)$; in addition, $b_p + b_c = b$.

To complete the system of equations for the hybrid system, a total of four relations at the splitting interface on each domain are needed for a unique solution. Two of these relations come by constraining the displacements at the interface [Eqs. (11*a*) and (12*a*)] as well as the rotations [Eqs. (11*b*) and (12*b*)]. The additional two relations are obtained by constraining the bending moments, M_y, and total shears, V_y, along the interface. This allows expression of any mismatch in the kinematic quantities *and* kinetic quantities at the interface, leading to the following system of equations that can be used to solve for the unknown boundary functions:

$$g^w_p(x, t) - f_w g^w_c(x, t) = 0 \tag{13a}$$

$$g^\theta_p(x, t) - f_\theta g^\theta_c(x, t) = 0 \tag{13b}$$

$$\hat{M}_{py}(x, b_p, t) - f_M \hat{M}_{c\tilde{y}}(x, b_c, t) = 0 \tag{13c}$$

$$\hat{V}_{py}(x, b_p, t) - f_V \hat{V}_{c\tilde{y}}(x, b_c, t) = 0 \tag{13d}$$

where

$$f_k = (1 + \varepsilon_k) e^{i\Omega d_k}, \qquad k \in \{w, \theta, M, V\} \tag{14}$$

such that $g^k_p = f_k g^k_c$, as introduced in Eq. (5). The expressions for M_y and V_y are determined, as usual, from the displacement (Timoshenko 1959) as

$$M_y = -D\left(\frac{\partial^2 w}{\partial y^2} + \nu \frac{\partial^2 w}{\partial x^2}\right) \tag{15a}$$

$$V_y = -D\left[\frac{\partial^3 w}{\partial y^3} + (1 - 2\nu)\frac{\partial^3 w}{\partial x^2 \partial y}\right] \tag{15b}$$

These expressions for the moments and shears are necessarily dependent on the Fourier coefficients Γ^w_{pm}, Γ^w_{cm}, Γ^θ_{pm}, and Γ^θ_{cm} and thus the system in Eqs. (13*a*) and (13*b*) can be used to uniquely solve for these coefficients. Ultimately, expressions for the displacements, rotations, bending moments, and shears in each domain, with known, locally introduced errors determined by ε_k and d_k, where k represents one of the quantities w, θ, M, or V, are determined.

The development to this point has been specific to the case of the simply supported plate subjected to a single edge moment. This was considered sufficient to elucidate the basic behavior of plate-like structures in the hybrid testing framework. Notwithstanding, many other boundary conditions and loading conditions are of practical interest and can be investigated using the same methodology. For general boundary and loading conditions, the primary change when doing so will be the need to replace Eq. (9) with more-general expansions, though in some cases they may still fall within the generalized Lévy framework. In the worst case setting, one will have to utilize the more slowly converging double trigonometric series method. The interface matching methodology, however, will remain the same.

Analysis

In the present context, hybrid simulation can be understood from a geometric point of view by considering the motion, $\mathbf{u}$, as being trajectories defined in a L^2 function space

$$L^2(\Omega) = \left\{ v : v \text{ is defined on } \Omega \text{ and } \int_\Omega v^2 d\mathbf{x} < \infty \right\} \tag{16}$$

where Ω = bounded domain in $\mathbb{R}^3$. It is known that $\mathbf{u} \in L^2(\mathcal{D})$, the restriction of $\mathbf{u}$ to $\mathcal{P}$ is $\mathbf{u}_p \in L^2(\mathcal{P})$, and the restriction of $\mathbf{u}$ to $\mathcal{C}$ is $\mathbf{u}_c \in L^2(\mathcal{C})$. In addition, $L^2(\mathcal{D}) = L^2(\mathcal{C}) \times L^2(\mathcal{P})$. The multiplication operation here is to be understood in the sense that functions over $\mathcal{C}$ and $\mathcal{P}$ are extend over the other domain with zero value and then summed. The trajectories given by $\mathbf{u}_c$ and $\hat{\mathbf{u}}_c$ (as well as $\mathbf{u}_p$ and $\hat{\mathbf{u}}_p$) differ from each other since the systems are, in general, different. By considering trajectories in $L^2(\mathcal{C})$ and $L^2(\mathcal{P})$ as components of generalized order pairs in $L^2(\mathcal{D})$ at each moment in time, trajectories from $L^2(\mathcal{C})$ and $L^2(\mathcal{P})$ can be combined into trajectories in $L^2(\mathcal{D})$, one for the reference system and one for the hybrid system. This difference gives the basis of the error analysis, which is measured using a space-time L^2-norm [Eqs. (17*a*) and (17*b*)].

Now consider the behavior of the hybrid system if a tracking error is introduced in the edge displacements at the interface. This could result in a system behavior as shown in Fig. 3(b). This is to be compared with the true system behavior shown in Fig. 3(a).

In order to assess the error in the hybrid system, L^2 space-time norms and seminorms are introduced, defined as

$$\|e_{pw}\|^2 = \int_\tau \int_{\mathcal{P}} (w - \hat{w}_p)^2 d\mathbf{x} d\tau,$$
$$\|e_{cw}\|^2 = \int_\tau \int_{\mathcal{C}} (w - \hat{w}_c)^2 d\mathbf{x} d\tau \tag{17a}$$

$$\|e_w\| = \sqrt{\|e_{pw}\|^2 + \|e_{cw}\|^2} \tag{17b}$$

L^2 norms of the rotation, $\theta_y = \partial w / \partial y$, bending moment, and shear errors are computed analogously to the displacement error norm. Perhaps more insightful are the relative norms

$$\|e_w\|_{\text{rel}} = \|e_w\| / \|w\|, \qquad \|e_\theta\|_{\text{rel}} = \|e_\theta\| / \|\theta_y\|,$$
$$\|e_M\|_{\text{rel}} = \|e_M\| / \|M_y\|, \qquad \|e_V\|_{\text{rel}} = \|e_V\| / \|V_y\| \tag{18}$$

In the case of an *unbounded* response, the quotients in Eq. (18) may numerically produce an artificially *bounded* error. For the subsequent analysis, norms evaluated at the precomputed natural

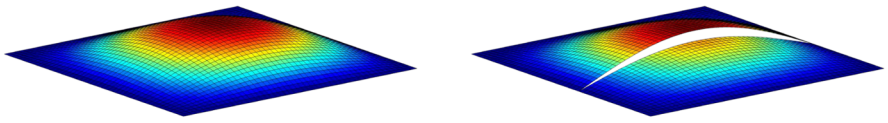

Fig. 3. Hybrid plate with a displacement gap: (a) perfect matching (no error); (b) forced incompatibility in displacement

frequencies of the plate (Leissa 1969) that produce the unbounded response are omitted. The following analysis will exclusively use these relative norms.

The integrals presented in Eqs. (17*a*) and (17*b*) can be evaluated analytically but this can be difficult to perform accurately due to the presence of hyperbolic trigonometric functions in Eq. (10) and in the analogous equations of the hybrid system. Instead, a high-order numerical quadrature routine is used (Kronrod 1965). This is simpler and does not compromise accuracy.

Validation of the Formulation

First, a validation of the proposed framework is presented by imposing perfect continuity between the $\mathcal{P}$ and $\mathcal{C}$ domains or in other words by setting the introduced error parameters $\varepsilon_k = 0$ and $d_k = 0$ in Eq. (14). Fig. 4 presents the relative global error, given by Eq. (18), for the displacement, rotation, bending moment, and shear. The parameter $\Omega = \omega/\bar{\omega}$ is the driving frequency of the harmonic excitation normalized by the first fundamental frequency of the system. The material parameters $E = 200$ GPa, $\nu = 0.3$, and $\rho = 7.9$ g/cm^3 are chosen to represent steel material, however, this analysis is not intended to be restricted by the selection of any particular material.

The expected errors are zero, however, values greater than the machine limit were observed for double precision. This loss of digits is attributed to the evaluation of the sums of hyperbolic terms in Eq. (10). The only source of error in this theoretical calculation comes from those introduced at the splitting interface, and to properly assess these errors, Fig. 4 can be considered as the baseline for zero error.

Effect of the Excitation Frequency

First, consider the effect of the excitation frequency on the global errors of the hybrid system relative to the true solution. Each curve in Fig. 5 presents a level of introduced error only in the displacement with fixed $d_k = 0.01$. Several observations are noted: (1) there is a strong tendency to accumulate errors in the vicinity of the natural frequencies of the system; (2) the error becomes somewhat unpredictable above the fundamental frequency; and (3) there are spikes of large errors not associated with natural frequencies, which will be discussed in the section on substructure excitation. Not all of the natural frequencies of the plate are excited due to the one-sided nature of the excitation (Fig. 2). The unpredictable nature of the errors at and above the first fundamental frequency indicates that hybrid tests with

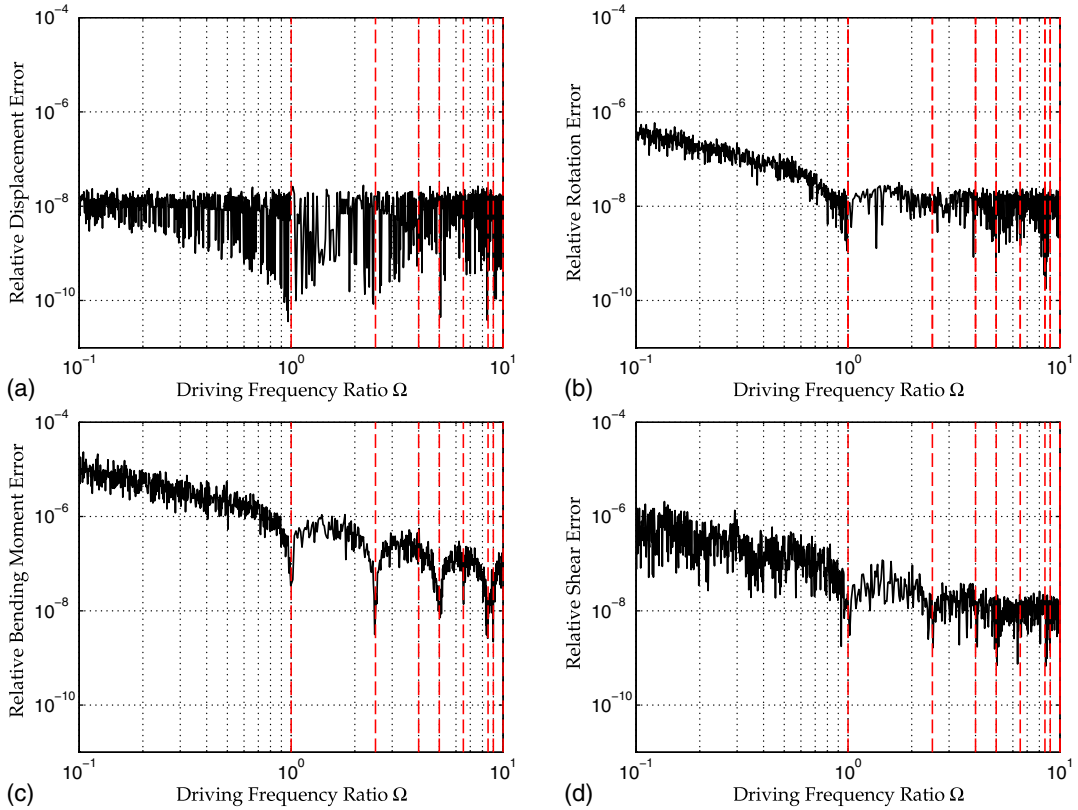

Fig. 4. Frequency sweep with zero introduced errors; vertical dashed lines indicate natural frequencies of the original (nonhybrid) system: (a) displacement; (b) rotation; (c) bending moment; (d) shear

J. Eng. Mech., 2016, 142(12): 04016093

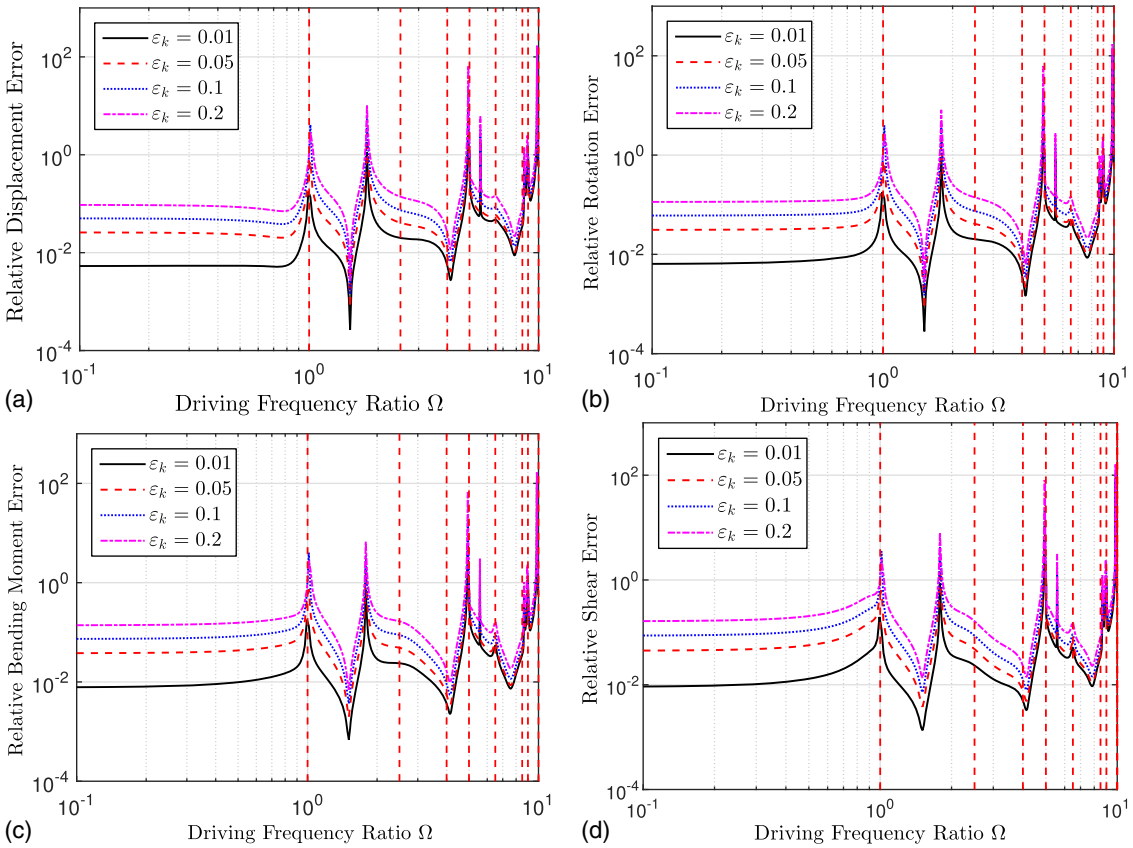

Fig. 5. Frequency sweep with $\varepsilon_k = \varepsilon_w$ errors in the displacement; vertical dashed lines indicate natural frequencies of the original (nonhybrid) system: (a) displacement; (b) rotation; (c) bending moment; (d) shear

dominant excitation frequencies above the first fundamental frequency or near the natural frequencies of the system may not be viable.

Effect of Error Type

The effect of introducing error in the rotation as well as the displacement is shown in Fig. 6(a) and the effect of introducing equal error in all four quantities is shown in Fig. 6(b). Due to the similarity of the different norms from Fig. 5, only results for the relative displacement error are presented. As expected, the global error increases as local error is introduced in more quantities at the interface. Interestingly, the large errors not associated with natural frequencies are absent when the only locally introduced errors are in the displacement and rotation.

Frequency-Dependent Errors

Making use of Eq. (6), the effect of frequency-dependent errors is demonstrated in Fig. 7 with $d_k = 0.01$, $k \in \{w, \theta, M, V\}$, and $\omega_{k0}/\omega = 4$. A clear upward trend shows that

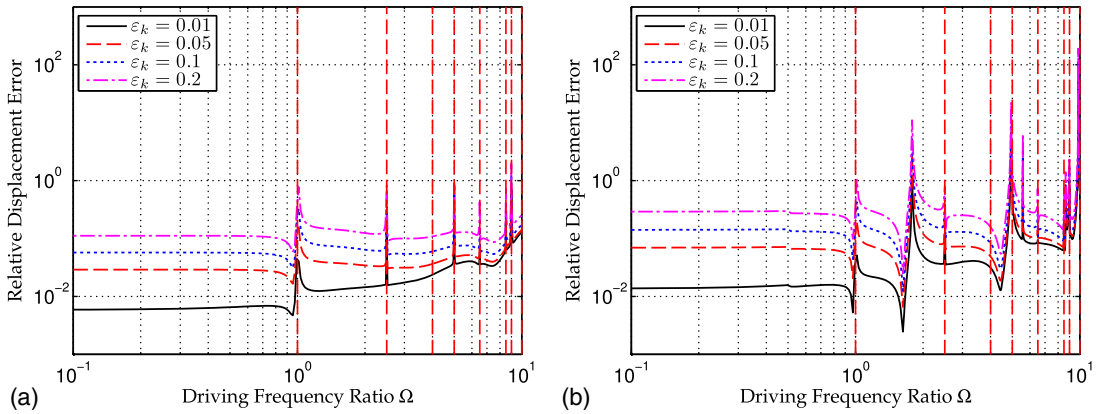

Fig. 6. Effect of different locally introduced errors at interface with $d_k = 0.01$: (a) local error in displacement and rotation; (b) local error in all interface quantities

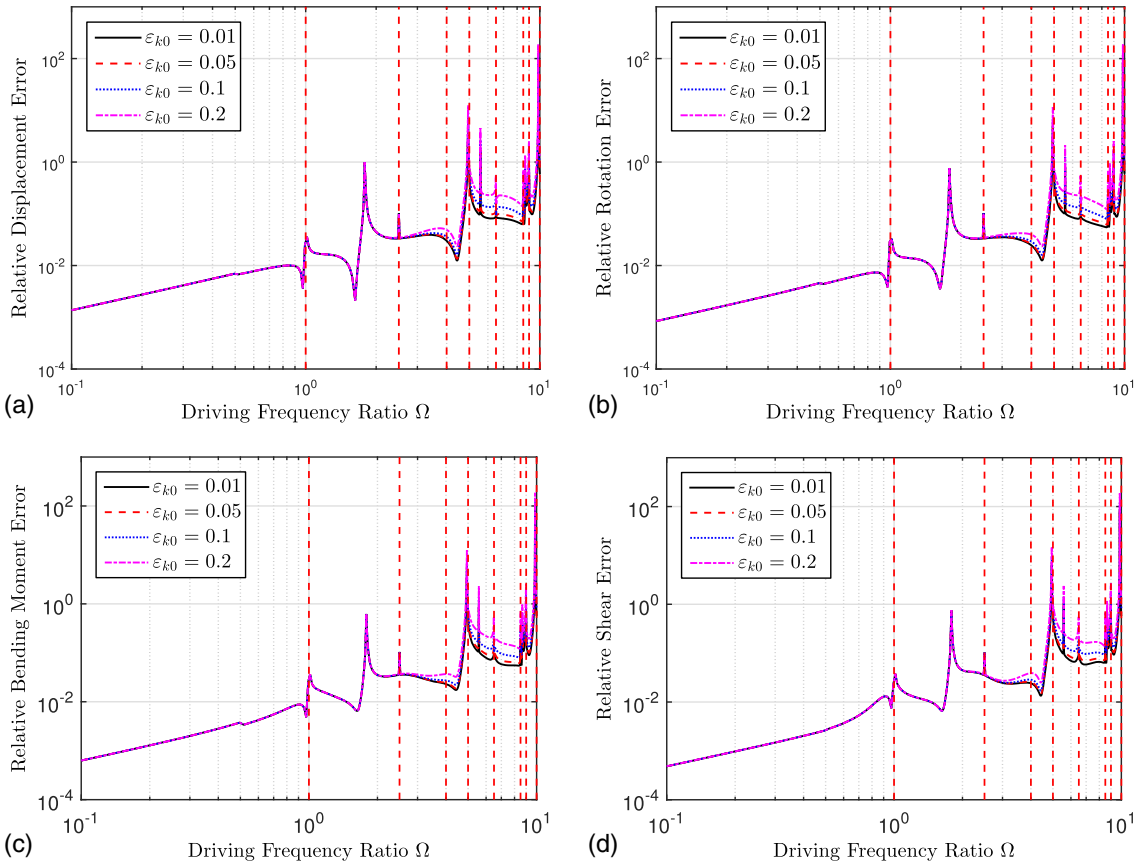

Fig. 7. Frequency dependent errors with $d_k = 0.01$ in all four boundary quantities: (a) displacement; (b) rotation; (c) bending moment; (d) shear

as the driving frequency grows, so does the global error. Not surprisingly, there is little difference in the global error of the various response quantities at low frequencies and the effect of ε_{k0} becomes significant only at higher normalized driving frequency.

Substructure Excitation

The error spikes not associated with a natural frequency of the plate are observed to be consistent with natural frequencies of one of the individual subplates created by the domain split. Fig. 8(a) presents

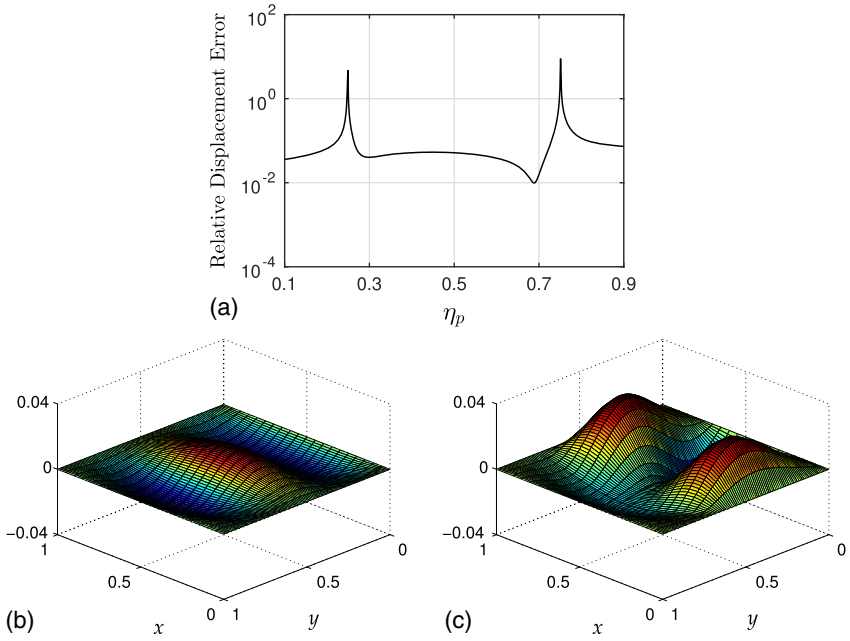

Fig. 8. Excitation of the subdomains in the presence of introduced errors with $\Omega = 5.58$: (a) sweep over domain separation with $\varepsilon_k = 5\%$; (b) true deformed shape of plate; (c) deformed shape of hybrid plate with $\varepsilon_k = 5\%$

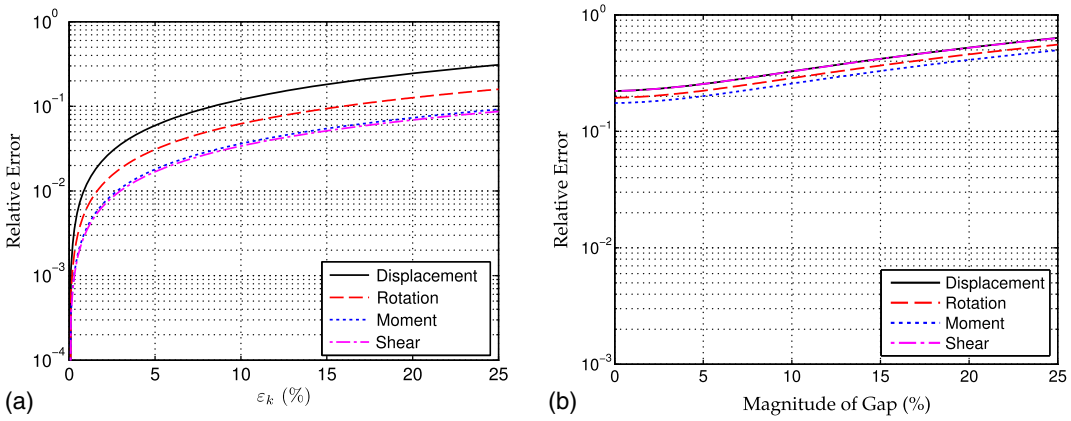

Fig. 9. Effect of varying ε_k with $\Omega = 0.5$: (a) $d_k = 0$; (b) $d_k = 0.05$

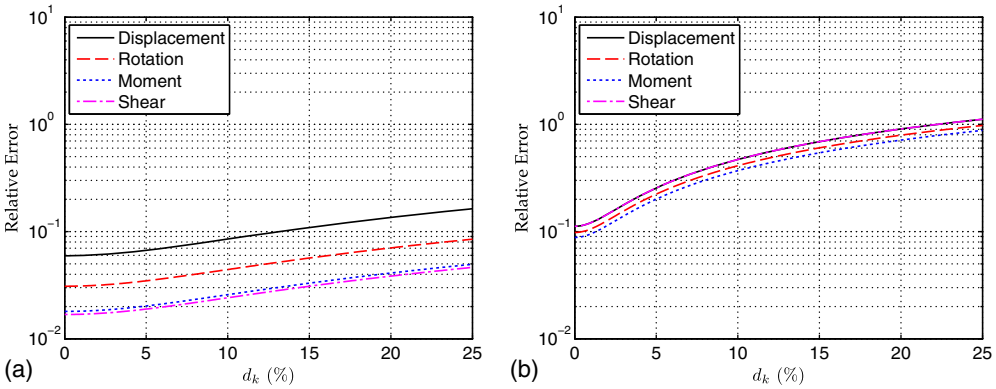

Fig. 10. Effect of varying d_k with $\varepsilon_k = 5\%$: (a) $\Omega = 0.5$; (b) $\Omega = 2.0$

the relative global displacement error versus the location where the separation is made for $\epsilon_k = 5\%$, ($k \in \{w, \theta, M, V\}$). The parameter η_p is defined as the location of separation normalized by the length of the plate orthogonal to the separation. A spike in the error is observed at one value of η_p and again at $1 - \eta_p$. This indicates that each subdomain is excited at resonance when its length takes on a critical value, which for the assigned boundary conditions of the substructures is consistent with a natural frequency (Leissa 1973). This is confirmed in Fig. 8(c) which demonstrates the $\mathcal{P}$-domain being excited at one of its individual eigenmodes as opposed to that of the real system. The small values in Fig. 4 indicate that these errors are not present when an interface error of zero value is introduced and thus this effect is only realized when a mismatch is introduced at the interface.

The implication of this is that the individual substructures can be excited independently during a hybrid test, particularly when the excitation is transient. This is consistent with studies that have demonstrated that delay in the control can lead to excitation of higher modes of the physical substructure (Shing and Mahin 1987). This behavior was also observed in experiments discussed by Bakhaty et al. (2014) when the effect of real-time HS with large computational substructures was investigated. In this case, components of the experimental set-up (the hydraulic oil-column in the actuator system) were observed to be excited. Although not intended as part of the physical substructure, the entire experimental set-up inevitably becomes part of the physical substructure, and in this case is excited, resulting in significant errors. Furthermore, when a different computational model is used, a different mode of the physical substructure is seen to be excited, leading to some errors.

Effect of the Magnitude and Phase of the Introduced Error

Fig. 9 presents the global displacement error versus ε_k introduced into all four boundary quantities with $d_k = 0$ and $d_k = 0.05$ at a fixed $\Omega = 0.5$. Fig. 10 presents the global displacement error versus d_k introduced into all four boundary quantities with $\varepsilon_k = 5\%$ and at two different excitation frequencies: $\Omega = 0.5$ in Fig. 10(a) and $\Omega = 2.0$ in Fig. 10(b). Each curve represents the global error in each of the response quantities as introduced by the norms in Eq. (18).

It is observed that the slightest introduction of the boundary error results in a rapid increase of the global error. However, the global error becomes quickly indifferent to increasing boundary errors. These results indicate that significant efforts to decrease the errors in the transfer system, particularly the reaction system of the test specimen, may result in little global error reduction of the hybrid system—especially in the presence of time-delay errors.

Spatial Distribution of Errors

The norms presented are useful for quantifying the overall behavior of the plate when a mismatch is introduced between the domains in the context of hybrid simulation. However, to understand the failure of given structural system, the local behavior is often of interest. Fig. 11 demonstrates the absolute difference between the true

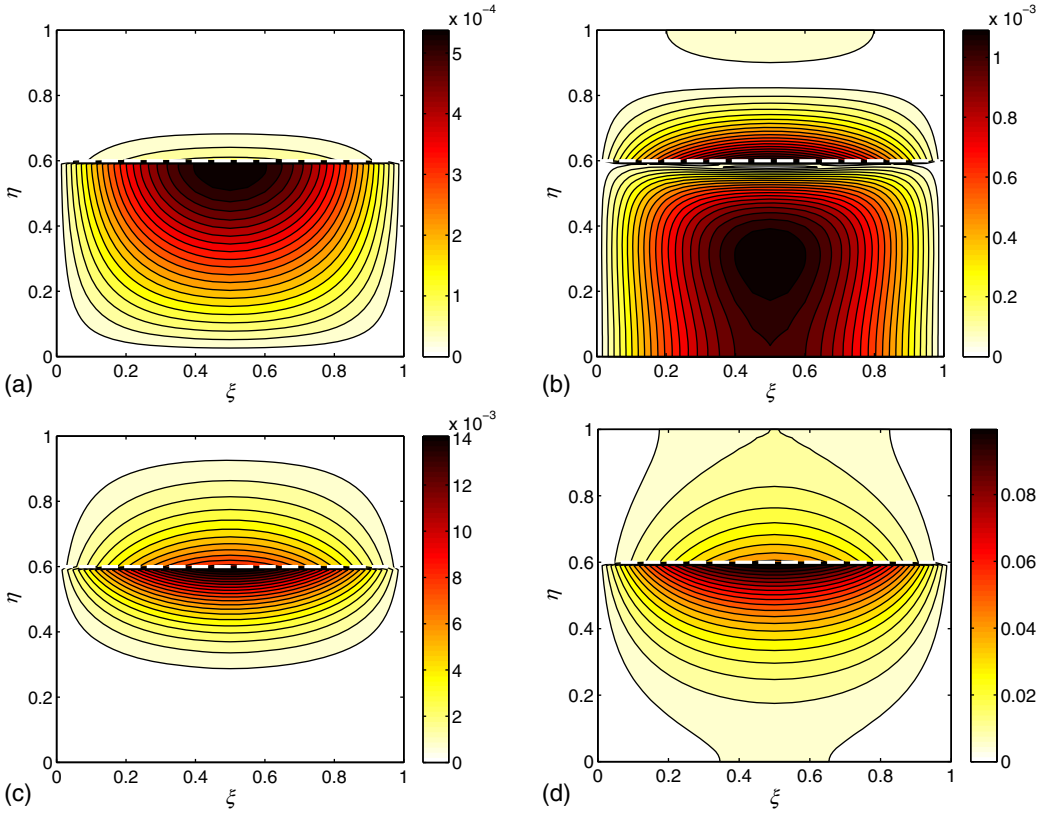

Fig. 11. Contour plots of absolute errors in plate at $\Omega = 0.5$ with $\varepsilon_k = 5\%$, $d_k = 0.01$ in all quantities. $\xi = x/a$ and $\eta = y/b$ are normalized coordinates; edge moment is at $\eta = 1$: (a) displacement error; (b) rotation error; (c) bending moment error; (d) shear error

(nonhybrid) solution and the hybrid solution at the time of maximum displacement with $\Omega = 0.5$. The location of the domain separation is indicated with a dashed line. A local error is introduced in displacement, rotation, bending moment, and shear at a magnitude of 5% and $d_k = 0.01$. The edge bending moment is applied at $\eta = y/b = 1$ (Fig. 2). There is a general trend observed that error accumulates around the interface where the local mismatch is introduced. The error propagates to the driving edge as well as the opposite edge for the rotation and the shear. Finally, there are observed errors in the regions of peak displacements, rotations, bending moments, and shears in the plate, indicating that locally introduced errors affect the global response of the system.

Conclusion

A theoretical framework for characterizing the errors in hybrid simulations was presented. The method was applied to a classical two-dimensional problem in continuum mechanics and the errors were presented with respect to analytically derived true solutions. The following are concluded from this study:

- The basic character of the two-dimensional continuum hybrid system is very similar to that of the one-dimensional hybrid system studied by Drazin et al. (2015);
- There are unpredictable errors at and above the first fundamental frequencies of the systems, with a large accumulation of errors near the resonant frequencies. This indicates that hybrid tests that excite the natural frequencies of a system may not be viable;
- The frequency of excitation plays a crucial role on the overall errors observed for the system; and
- Efforts to further decrease the errors in the transfer system may result in disappointingly little reduction in the global errors. In the present two-dimensional study, it is further found that
- Frequency-dependent errors based on the logistic model in the transfer system lead to linearly increasing errors on the log-log scale;
- Substructures of a hybrid test respond to excitation dominated by their individual natural frequencies in addition to the natural frequencies of the real system. These results have been corroborated by experiments (Mosalam et al. 2012); and
- Locally introduced errors propagate to peak deformations and boundary quantities; they do not necessarily remain localized as one would expect from a naïve Saint Venant effect argument.

Acknowledgments

This research was financially supported by National Science Foundation Award Number CMMI-1153665. Any opinions, findings, and conclusions or recommendations expressed are those of the authors and do not necessarily reflect those of the National Science Foundation.

References

Ahmadizadeh, M., Mosqueda, G., and Reinhorn, A. M. (2008). "Compensation of actuator delay and dynamics for real time hybrid structural simulation." *Earthquake Eng. Struct. Dyn.*, 37(1), 21–42.

Bakhaty, A. A., Govindjee, S., and Mosalam, K. M. (2014). "Theoretical development of hybrid simulation applied to plate structures." *Rep. No.*

PEER Report 2014/02, Pacific Earthquake Research Center, Univ. of California, Berkeley, CA.
Conte, J. P., and Trombetti, T. L. (2000). "Linear dynamic modeling of a uni-axial shaking table system." *Earthquake Eng. Struct. Dyn.*, 29(9), 1375–1404.
Drazin, P. L., Govindjee, S., and Mosalam, K. M. (2015). "Hybrid simulation theory for continuous beams." *J. Eng. Mech.*, 10.1061/(ASCE)EM.1943-7889.0000909, 04015005.
Elkhoraibi, T., and Mosalam, K. M. (2007). "Towards error-free hybrid simulation using mixed variables." *Earthquake Eng. Struct. Dyn.*, 36(11), 1497–1522.
Gorman, D. J., and Sharma, R. (1976). "A comprehensive approach to the free vibration analysis of rectangular plates by use of the method of superposition." *J. Sound Vib.*, 47(1), 126–128.
Graff, K. F. (1975). *Wave motion in elastic solids*, Oxford University Press, London.
Günay, S., and Mosalam, K. M. (2014). "Seismic performance evaluation of high voltage disconnect switches using real-time hybrid simulation—II: Parametric study." *Earthquake Eng. Struct. Dyn.*, 43(8), 1223–1237.
Günay, S., and Mosalam, K. M. (2015). "Enhancement of real-time hybrid simulation on a shaking table configuration with an advanced control method." *Earthquake Eng. Struct. Dyn.*, 44(5), 657–675.
Horiuchi, T., Inoue, M., Konno, T., and Namita, Y. (1999). "Real-time hybrid experimental system with actuator delay compensation and its application to a piping system with energy absorber." *Earthquake Eng. Struct. Dyn.*, 28(10), 1121–1141.
Horiuchi, T., and Konno, T. (2001). "A new method for compensating actuator delay in real-time hybrid experiments." *Philos. Trans. R. Soc. Math. Phys. Eng. Sci.*, 359(1786), 1893–1909.
Igarashi, A., Seible, F., and Hegemeier, G. A. (1992). "Testing of full scale shear wall structures under seismic load." *Proc., 10th World Conf. on Earthquake Engineering*, A.A. Balkema, Rotterdam.
Kronrod, A. S. (1965). *Nodes and weights of quadrature formulas: Sixteen-place tables*, Consultants Bureau New York, New York.
Leissa, A. W. (1969). *Vibration of plates*, Acoustical Society of America, Columbus, OH.
Leissa, A. W. (1973). "The free vibration of rectangular plates." *J. Sound Vib.*, 31(3), 257–293.
Mosalam, K. M., and Günay, S. (2014). "Seismic performance evaluation of high voltage disconnect switches using real-time hybrid simulation—I: System development and validation." *Earthquake Eng. Struct. Dyn.*, 43(8), 1205–1222.
Mosalam, K. M., Moustafa, M. A., Günay, M. S., Triki, I., and Takhriov, S. (2012). "Seismic performance of substation insulator posts for vertical-break disconnect switches." *Rep. No. CEC-500-2012*, California Energy Commission, Sacramento, CA.
Nakashima, M. (2001). "Development, potential, and limitations of real-time online (pseudo-dynamic) testing." *Philos. Trans. R. Soc. Math. Phys. Eng. Sci.*, 359(1786), 1851–1867.
Richards, F. J. (1959). "A flexible growth function for empirical use." *J. Exp. Bot.*, 10(2), 290–301.
Schellenberg, A. H. (2008). "Advanced implementation of hybrid simulation." Ph.D. thesis, Univ. of California, Berkeley, CA.
Shing, P. S. B., and Mahin, S. A. (1984). "Pseudodynamic test method for seismic performance evaluation: Theory and implementation." *Rep. No. 190644*, Earthquake Engineering Research Center, Berkeley, CA.
Shing, P. S. B., and Mahin, S. A. (1987). "Elimination of spurious higher-mode response in pseudodynamic tests." *Earthquake Eng. Struct. Dyn.*, 15(4), 409–424.
Takanashi, K., Udagawa, K., Seki, M., Oakada, T., and Tanaka, H. (1975). "Nonlinear earthquake response analysis of structures by a computer-actuator on-line system." *Bulletin of Earthquake Resistant Structure Research Center*, Univ. of Tokyo, Tokyo, 1–17.
Taylor, R. L., and Govindjee, S. (2004). "Solution of clamped rectangular plate problems." *Commun. Numer. Methods Eng.*, 20(10), 757–765.
Thewalt, C. R., and Mahin, S. A. (1987). "Hybrid solution techniques for generalized pseudodynamic testing." *Technical Rep.*, Earthquake Engineering Research Center, Berkeley, CA.
Timoshenko, S. (1959). *Theory of plates and shells*, 2nd Ed., McGraw-Hill, Blacklick, OH.